Original Research Article

DCE-MRI assessment of response to neoadjuvant SABR in early stage breast cancer: Comparisons of single versus three fraction schemes and two different imaging time delays post-SABR

Matthew Mouawad [a,*], Heather Biernaski [b], Muriel Brackstone [a,b,c,d], Michael Lock [c,e], Brian Yaremko [c,e], Olga Shmuilovich [b,d,f], Anat Kornecki [b,d,f], Ilanit Ben Nachum [b,d,f], Giulio Muscedere [b,d,f], Kalan Lynn [b,c,d], Frank S. Prato [a,b,d,f], R. Terry Thompson [a,b], Stewart Gaede [a,b,c,e], Neil Gelman [a,b,f]

[a] Medical Biophysics, Western University, London, Ontario, Canada
[b] Lawson Health Research Institute, London, Ontario, Canada
[c] London Health Sciences Centre, London, Ontario, Canada
[d] St. Joseph's Health Care, London, Ontario, Canada
[e] Department of Oncology, Western University, London, Ontario, Canada
[f] Department of Medical Imaging, Western University, London, Ontario, Canada

ARTICLE INFO

ABSTRACT

Purpose: To determine the effect of dose fractionation and time delay post-neoadjuvant stereotactic ablative radiotherapy (SABR) on dynamic contrast-enhanced (DCE)-MRI parameters in early stage breast cancer patients.

Materials and methods: DCE-MRI was acquired in 17 patients pre- and post-SABR. Five patients were imaged 6–7 days post-21 Gy/1fraction (group 1), six 16–19 days post-21 Gy/1fraction (group 2), and six 16–18 days post-30 Gy/3 fractions every other day (group 3). DCE-MRI scans were performed using half the clinical dose of contrast agent. Changes in the surrounding tissue were quantified using a signal-enhancement threshold metric that characterizes changes in signal-enhancement volume (SEV). Tumour response was quantified using K^{trans} and v_e (Tofts model) pre- and post-SABR. Significance was assessed using a Wilcoxin signed-rank test.

Results: All group 1 and 4/6 group 2 patients' SEV increased post-SABR. All group 3 patients' SEV decreased. The mean K^{trans} increased for group 1 by 76% ($p = 0.043$) while group 2 and 3 decreased 15% ($p = 0.028$) and 34% ($p = 0.028$), respectively. For v_e, there was no significant change in Group 1 ($p = 0.35$). Groups 2 showed an increase of 24% ($p = 0.043$), and Group 3 trended toward an increase (23%, $p = 0.08$).

Conclusion: Kinetic parameters measured 2.5 weeks post-SABR in both single fraction and three fraction groups were indicative of response but only the single fraction protocol led to enhancement in the surrounding tissue. Our results also suggest that DCE-MRI one-week post-SABR may be too early for response assessment, at least for single fraction SABR, whereas 2.5 weeks appears sufficiently long to minimize confounding acute effects.

* Corresponding author at: 800 Commissioners Road East, Room A4-841, P.O. Box 5010, STN B, London, ON N6A 5W9, Canada.
E-mail addresses: mmouawad@uwo.ca (M. Mouawad), Heather.Biernaski@LawsonResearch.Com (H. Biernaski), Muriel.Brackstone@lhsc.on.ca (M. Brackstone), Michael.Lock@lhsc.on.ca (M. Lock), Brian.Yaremko@lhsc.on.ca (B. Yaremko), Olga.Shmuilovich@lhsc.on.ca (O. Shmuilovich), Anat.Kornecki@sjhc.london.on.ca (A. Kornecki), Ilanit.BenNachum@sjhc.london.on.ca (I. Ben Nachum), Giulio.Muscedere@sjhc.london.on.ca (G. Muscedere), Kalan.Lynn@lhsc.on.ca (K. Lynn), prato@lawsonimaging.ca (F.S. Prato), thompson@lawsonimaging.ca (R.T. Thompson), Stewart.Gaede@lhsc.on.ca (S. Gaede), ngelman@lawsonimaging.ca (N. Gelman).

1. Introduction

The current standard of breast conserving therapy for early stage breast cancer patients is a lumpectomy followed by whole breast radiotherapy delivered over 3–6 weeks [1]. This treatment time is prohibitively long for many patients [1,2]. Accelerated partial breast irradiation (APBI) is being investigated to reduce treatment time by treating local to the tumour [3] while attempting to maintain the same efficacy as the current standard. The

treatment volume can be further reduced by treating before surgery, as in this case, the treatment volume includes only the intact tumour and, thus, does not include the surgical margins [4]. This allows large doses to be delivered per fraction and facilitating the use of stereotactic ablative radiotherapy (SABR). With pre-surgical radiotherapy it becomes possible to use imaging to assess the physiological effects of the radiation and investigate potential tumour response biomarkers. Determination of tumour control at an early stage could potentially allow patient-specific radiotherapy adaptation.

It has been shown that microvascular damage from radiotherapy plays a key role in tumour regression [5,6]. Dynamic contrast enhanced (DCE) MRI provides a means to assess microvasculature function and potential damage. Parameters extracted from DCE-MRI include the rate at which a gadolinium contrast agent exits capillaries into the extracellular-extravascular space (K^{trans}) and the volume of the extracellular, extravascular space (v_e). Using these metrics we can non-invasively assess response to the SABR treatment [7].

Pre-clinical and clinical studies have demonstrated early vs late changes in tumour response parameters related to blood flow and vessel permeability. Early changes have been attributed to acute inflammatory reactions which can cause increased vessel permeability, and endothelial cell death within irradiated volumes [5,6,8]. Determination of the optimal time post-radiotherapy for DCE-based assessment of response without confounding acute effects remains an unanswered question.

In addition to the effect of high doses of radiation within the tumour it is important to consider the influence of irradiation on the surrounding tissue, which has been seldom studied in humans. Pre-clinical studies have suggested there may exist a threshold dose (8–12 Gy) above which a cascade of events leads to endothelial apoptosis in normal vasculature [6,9–12].

To our knowledge, only one study has investigated DCE-MRI after SABR in the context of breast cancer [13]. DCE-MRI parameters (K^{trans}, v_e, area under enhancement curve) were quantified one week following single-fraction SABR (15, 18, or 21 Gy). Measurements were limited to region-of-interest enhancement curves (rather than voxel-wise curves) for the gross, clinical, and planning target volumes (GTV, CTV, PTV). However, no values of K^{trans} or v_e for the GTV, which most closely relates to the tumour region, were reported. Finally, the authors used an arterial input function proposed by Weinmenn in 1984 [14] that has shown to have poor performance [15].

In this work we investigated the utility of DCE-MRI measures to detect early response to SABR in a cohort of patients who had received a single high dose (21 Gy/1fraction) and a cohort who had received a fractionated a fractionated scheme (30 Gy/3fractions every other day), with both of these cohorts imaged at approximately 2.5 weeks following SABR. While these two schemes provide approximately equivalent tumour cell killing according to the linear quadratic model and universal survival curves [2], we wanted 1) to verify that the two schemes demonstrate a measurable tumour response as assessed by DCE-MRI and 2) to determine if DCE-MRI measures are consistent with expectations that the fractionated scheme would lead to a differential effect in the surrounding tissue due to the higher biologically effective dose in the single fraction scheme in this tissue. In addition, we also acquired and analyzed DCE images from a cohort of patients scanned at approximately 1 week post single high dose SABR (21 Gy/1fraction), allowing us to compare the single fraction DCE-MRI based response at two time points post SABR. This information is important in developing a protocol for monitoring SABR response as one would hope to monitor response as early as possible while avoiding potential confounding factors (e.g., inflammatory changes). To investigate tumour response, we applied the

Tofts pharmacokinetic model to assess pre to post-SABR changes within the tissue enhancing in the pre-SABR scan. To investigate the influence of SABR on tissue surrounding the tumour, the changes in enhancing tissue volume from pre to post-SABR were quantified. All scans were performed using only half the clinical dose of MRI contrast agent.

2. Materials and methods

2.1. Patients

Images were acquired as part of a phase I/II clinical trial called SIGNAL involving early stage breast cancer patients [2]. At the time of tumour core biopsy, a surgical clip was placed adjacent to or within the tumour. Patient data was acquired from two cohorts of patients and patient demographics are given in Table 1. The first cohort is from patients treated with neoadjuvant 21 Gy/1 fraction SABR and who received lumpectomy within approximately 1-week of SABR. The second cohort were from a protocol where patients were randomly assigned to either 21 Gy/1 fraction or 30 Gy/3 fractions every other day, with both groups receiving lumpectomy at approximately 3 weeks post-SABR. All patients received MRI (including DCE-MRI) prior to SABR for tumor delineation in SABR planning. In addition, patients were offered the opportunity to participate in a sub-study which involved post-SABR MRI as close to the lumpectomy as possible. The protocols, including post-SABR MRI, were approved by the Western University Human Subjects Research Ethics Board.

2.2. Image acquisition

Images were acquired on a Siemens Biograph mMR 3T-PET/MRI system (Siemens Medical, Erlangen, Germany) with a four channel prone breast coil [16].

Prior to contrast injection, native T_1 relaxation time (T_{10}) maps were generated using the variable flip angle (VFA) method [17] for conversion of signal to concentration [7]. B_1 maps were acquired to determine the true flip angle for both T_{10} mapping and DCE-MRI [7]. Due to a scanner upgrade, two different sequences for B_1 quantification were used- the Actual Flip Angle (AFI) [18] and the "slice-selective pre-conditioning RF pulse" (SS-Pre) [19] methods. Imaging parameters for both methods are provided in Table 2. T_{10} maps were reconstructed in MATLAB v. 2018a (Mathworks Inc., Natick, MA).

Three-dimensional fat suppressed fast low angle shot (FLASH) images were acquired with field-of-view = 38x38cm, slab thickness = 13.4 cm, time of acquisition = 20 s using 6/8 partial Fourier in two directions and an acceleration factor of two. The DCE series included a pre-contrast and 28-post gadobutrol (Gadavist®) contrast injection images using a dose of 0.05 mmol/kg (half the clinical dose), and an injection rate of 0.75 ml/s for patients in the DCE-MRI sub-study [20]. Immediately after injection but prior-to post-contrast images, single slice half-Fourier acquisition single-shot turbo spin echo (HASTE) images, positioned at the arch of the aorta were acquired for approximately 19 s.

2.3. Image registration

To correct for intra-session motion, DCE images were deformably registered to the mid-time point post-contrast image using 3DSlicer v4.8.0 [21–23]. To correct for patient movement between the B_1 and T_{10} mapping scans relative to the DCE-MRI, deformable registration was performed using MIM (v6.8.5, MIM Software, Cleveland, USA) and its multi-modality metric [24,25].

Following intra-session registration, a post- to pre-radiotherapy registration was performed. The post-radiotherapy, pre-contrast

Table 1
Study/patient information, image timing and SABR treatment scheme separated by group. Note that for the 3 fraction patients, imaging time post-treatment is the time delay from the conclusion of radiation therapy to the MRI scan.

	# Patients	Dose Scheme	Median (Range) Imaging Time Post-treatment (days)	Breast affected	Mean Age
Group 1	5	21 Gy/1FX	6 (6–7)	3L/2R	72
Group 2	6	21 Gy/1FX	16 (16–19)	3L/3R	69
Group 3	6	30 Gy/3FX	16 (15–18)	3L/3R	69

FX = fraction, L / R = Left or right sided breast affected

Table 2
Acquisition Parameters for MRI sequences used in this study.

Acquisition	Nominal FA	TR (ms)	TE (ms)	Spatial Resolution (mm)	Interpolated voxel size (mm)
HASTE	10°	489.6/521.4	1.16/1.36	$1.4 \times 2.0 \times 5$	$1.4 \times 1.4 \times 5$
DCE-MRI	15°	4.1	1.5	$1.0 \times 2.1 \times 2.1$	$1.0 \times 1.0 \times 1.2$
VFA (T_1 map)	5 or 6 FAs (1° to 17°)	4.9 or 5.1	1.9 or 2.5	$1.0 \times 1.1 \times 2.11$ or $1.0 \times 2.1 \times 2.0$	$1 \times 1 \times 1.2$ or $1.0 \times 1.0 \times 1.0$.
AFI B_1 Map	50°	TR1 = 20 TR2 = 100	2.46	$2.4 \times 4.0 \times 2.4$	$2.4 \times 2.4 \times 2.4$
SS-Pre B_1 Map	80°	10,000	2.0	$5.94 \times 5.94 \times 5$	N/A

VFA = variable flip angle, AFI B_1 = actual flip angle B_1 mapping sequence, SS-PRE B_1 = slice-selective pre-conditioning RF pulse B_1 mapping sequence

image was deformably registered to the pre-radiotherapy pre-contrast image (MIM v6.8.5, MIM Software, Cleveland, USA).

2.4. Analysis

2.4.1. Signal enhancement volume

The purpose of this analysis was to assess the change in the volume of enhancement pre- to post-SABR. A 3D rectangular cuboid centered on the tumour and sized to encompass all visibly enhancing tissue (excluding skin) was manually drawn on the 9th post-contrast (3.3 min post-injection) DCE-MRI image in the pre-radiotherapy setting. The same sized cuboid was used for the post-radiotherapy data for a given patient. A signal-enhancement map was calculated by dividing the 9th post-contrast DCE-MRI image by the pre-contrast for both the pre and post-SABR data. Within the cuboid, the signal-enhancement volume ≥ signal enhancement thresholds ranging from 1 to 5 with increments of 0.01 was calculated, generating threshold vs signal enhancement volume curves. The area under these curves (AUC) was calculated (higher values indicating greater volume of enhancement). The percent change in AUC from pre- to post-SABR was calculated and used for group comparisons.

2.4.2. Tumour segmentation

The tumour was automatically segmented in the pre-SABR DCE-MRI images (Fig. 1A). Initial filtering was performed using Otsu's segmentation method [26] on a subtraction image (last post-contrast – pre-contrast). K-means clustering using three clusters was applied using five features: 1–3) XYZ spatial position, 4) the entropy of a voxel (MATLAB entropyfilt with 9,9 neighbourhood) [27], and 5) the signal intensity of a mean subtraction image (average of the last 5 post-contrast images subtracting the pre-contrast image). Each feature was normalized to have a mean of zero and standard deviation of 1 [28]. The post- to pre-SABR deformation field was applied to the pre-SABR tumour contour resulting in a post-SABR tumour contour (Fig. 1B).

2.4.3. Kinetic analysis

Using the tumour contour, the surgical clip was automatically segmented and removed followed by a 2 pixel in-plane erosion to remove partial volume voxels. The average B_1 and T_{10} over each tumour contour was calculated. Changes in B_1 and T_{10} pre- to post-SABR data were compared to determine if differences were statistically significant. Following this, the average across all patients was calculated, and this population-derived T_{10} [29] was used to
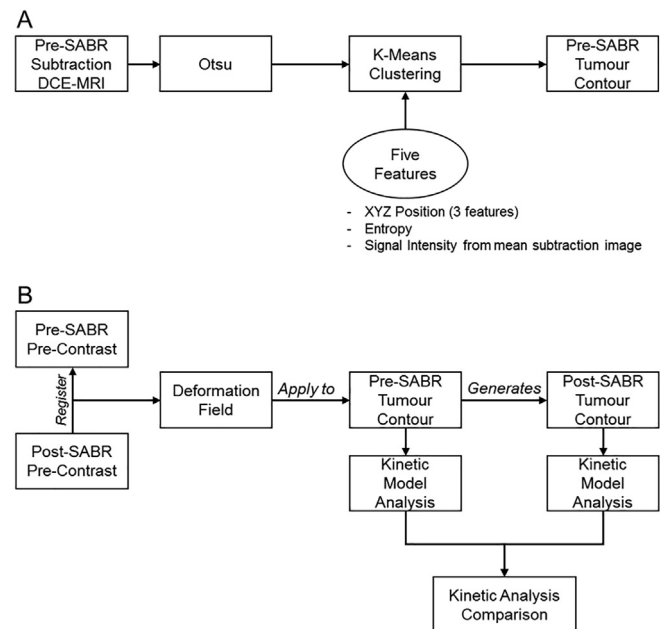
Fig. 1. Schematic representation of the process in generating the (A) pre-SABR tumour contour and (B) post-SABR tumour contour. The pre-SABR contour was generated using a k-means clustering algorithm with 5 features. Following this, the post-SABR pre-contrast image was registered to the pre-SABR pre-contrast image and the deformation field was applied to the pre-SABR contour.

convert signal enhancement to concentration [7] using a relaxivity of 4.5 s^{-1} mM^{-1} [30].

The Tofts model [31] was applied voxel-by-voxel to concentration curves within the tumour contour using a population-derived arterial input function (AIF) [32], with amplitude adjusted to our dose. An adjustable fit parameter was included to account for the delayed bolus arrival with a lower time bound set using contrast agent arrival time at the aortic arch from the HASTE images. K^{trans} and v_e were extracted from the model fit. For each tumour, the mean (K^{trans}, v_e) and standard deviation (σK^{trans}, σv_e) of the parameters were calculated. The median absolute difference method [33] was used to remove v_e values that were outliers in each tumour. The rationale for outlier removal was to eliminate the influence of very high (unphysical) voxel values of v_e on the contour mean value of v_e. These high values occurred in voxels with slow washout kinetics for which the acquisition time was

not sufficient to accurately measure k_{ep}, often leading to extremely low k_{ep} values and hence high v_e values ($v_e = K^{trans}/k_{ep}$). Changes in kinetic parameters between pre- and post-SABR scans are reported as the percent change in the mean of the group.

2.4.4. Statistical analysis

A Wilcoxon signed-rank test was used to test for significant within-subject changes between pre- and post-SABR kinetic parameters (α = 0.05, SPSS Inc. v25.0 Chicago). For T_{10}, differences between pre- and post-SABR in group 1 could not be tested in 3 out of 5 patients due to small tumours as well as clip placement. Finally, for the signal enhancement volume and kinetic parameters, the percent change from pre- to post-SABR was calculated per patient, and the groups were compared with each other using a Mann-Whitney U test.

3. Results

A total of 17 patients were recruited for this DCE-MRI study. The first 5 patients were from the first cohort (21 Gy/1 fraction, lumpectomy at approximately 1 week post SABR), and 12 patients from the second cohort (lumpectomy at approximately 3 weeks post-SABR). Six patients received 21 Gy/1 fraction and 6 patients received 30 Gy/3 fractions. Patients are categorized into three groups as indicated in Table 1. The mean (standard deviation) time between initial biopsy and pre-SABR imaging was 35 (9) days. The mean time between SABR and DCE-MRI for groups 2 and 3 was 17 days which was substantially longer than for group 1 (6 days).

Table 3 shows signal enhancement volume AUC percent change values and the pre-SABR contour volume for each patient by group. The AUC increased in all group 1 patients and in 4/6 group 2 patients though we found a significance difference (p = 0.018) in the percent changes in AUC between these two groups. On the other hand, group 3 patients all showed decreases in the percent change of AUC, and these values were different than those of groups 1 and 2 (p = 0.006 and 0.016, respectively). Fig. 2a shows subtraction images from three representative patients for the three groups pre and post-SABR, demonstrating the increased enhancement in the tissue surrounding the tumour for single fraction patients. Fig. 2b shows representative signal enhancement threshold volume versus threshold curves.

Regarding T_{10}, the average ± standard deviation for pre- and post-SABR was 1571 ± 264 ms and 1656 ± 204 ms, respectively.

This difference was not significant. Therefore, the average of these two values (1613 ms) was applied for conversion of enhancement signal to contrast concentration.

Fig. 3a and 3b illustrate pre- to post-SABR changes in the mean values of K^{trans} and v_e, respectively, referring to the mean across each contoured region. Mean K^{trans} values for group 1 increased 76% (p = 0.043) but decreased for groups 2 and 3 by 15% (p = 0.028) and 34% (p = 0.028), respectively. Mean values of v_e increased 25% (p = 0.046) for group 2 and showed a trend to increase of 32% (p = 0.075) for group 3, but did not reach significance. Group 1 showed no significant change (p = 0.138).

Fig. 3c and 3d illustrate pre to post-SABR changes in σK^{trans} and σv_e, respectively, representing the spatial variability across contoured regions. For group 1, σK^{trans} increased 100% (p = 0.043), but decreased by 31% (p = 0.028) for group 3. No significant change of σK^{trans} was found for group 2 (p = 0.173). For σv_e, group 2 and 3 showed increases of 36% (p = 0.046) and 113% (p = 0.028), respectively. There was no significant change in σv_e for group 1 (p = 0.225).

When comparing groups 1 and 2, with regard to the pre- to post-SABR changes in parameters, we found significant difference between groups only for K^{trans} (p = 0.006) and σK^{trans} (p = 0.011). Regarding K^{trans}, there was a 77% increase for group 1 and 15% decrease for group 2. For σK^{trans} there was a 103% increase for group 1 and 16% decrease for group 2.

4. Discussion

In this study, we investigated changes in quantitative DCE-MRI parameters post-SABR with two different fractionation schedules and two different imaging times for the single fraction scheme. Our results show a differential tumour response depending on time-delay post-SABR. In addition, we found a signal-enhancement volume increase post-single fraction SABR that was also seen 2.5 weeks post-SABR in most patients. To our knowledge, no study has reported this signal enhancement volume change (Fig. 2, Table 3).

In the context of previous studies, our results suggest that 2.5 weeks post-SABR is sufficient in order to minimize acute transient inflammatory effects. In other sites, it has been shown that at short times post-stereotactic radiotherapy (~1–2 weeks post-therapy), there are transient increases in K^{trans} following therapy, primarily attributed to endothelial cell death and permeability increases accompanying acute inflammatory effects [5,13,34–38]. A recent early stage breast cancer study [13] found significant increases in the initial area under an enhancement curve for the entire GTV at one-week post-single dose SABR. However, when assessing response at later times (>1month) in other cancer sites, decreases in K^{trans} were associated with pathologically complete response [39–41]. Two of these reports [39,41] also indicated that decreases in σK^{trans} was indicative of response.

Our results suggest that the three-fraction scheme provides an equivalent or stronger response than the single fraction scheme at three weeks post-SABR. The magnitude of change in the mean K^{trans} was greater for the three-fraction group compared to the single fraction group at three weeks post-SABR (34% vs 15%). However, only the single fraction scheme led to an increase in enhancement volume for the surrounding tissue for some patients (4/6). We speculate that the absence of increased enhancement for the three fraction group is related to reduced radiation damage to the surrounding tissue due to repair mechanisms as per radiobiological theory. We suspect that this differential effect on surrounding tissue is related to an endothelial cell death dose threshold which has been hypothesized to be on the order of 8–12 Gy delivered in a single dose [6,9,10,42–45]. With endothelial cell death,

Table 3
Pre-SABR contour volume and pre to post SABR percent change for signal enhancement area under the curve (AUC) for each patient in the different groups. Bold indicates an increase in the AUC value from pre- to post-SABR.

	Patient #	Pre-SABR Contour Volume (cm^3)	Percent change (%) for Signal Enhancement AUC
Group 1	1	0.07	**1932**
	2	2.22	**598**
	3	0.60	**295**
	4	0.49	**64**
	5	0.11	**1829**
Group 2	6	1.23	**180**
	7	0.72	**52**
	8	1.27	−18
	9	0.33	−31
	10	1.93	**144**
	11	0.47	**45**
Group 3	12	0.66	−42
	13	0.62	−28
	14	2.26	−77
	15	1.37	−14
	16	0.57	−87
	17	0.77	−40

Fig. 2. Subtraction images (A) and associated signal enhancement threshold vs volume curves (B) from representative patients for each of the three groups. The slices are approximately through the center of the tumour. The pink outline represents the skin/air interface. The single fraction images show clear evidence of an increase in the signal enhancement volume local to the tumour following SABR, and this is not seen in the 30 Gy/3 fraction patient. (For interpretation of the references to colour in this figure legend, the reader is referred to the web version of this article.)

gadolinium contrast would be freer to diffuse into the extra-cellular, extra-vascular space and result in enhancement outside the tumour. Long-term follow-up studies are needed to understand the long-term implications of this in terms of post-radiotherapy toxicities.

The application of v_e as a metric for response assessment remains unclear. It is expected that vascular and cellular death would lead to increases in v_e [5,13]. We found a significant increase in group 2 and a trend to increase in group 3, but not for group 1 (one-week post-SABR). However, Wang et al. [13] showed a significant increase in v_e at 1 week post-SABR for the PTV and CTV, but did not report v_e for the GTV which most closely corresponds to the volumes used in our study. On the contrary, Winter et al. [36] found significant decreases in v_e at 20 days post stereotactic radiosurgery for brain metastases. Furthermore, most studies do not find a significant change in v_e following therapy [34–36,39,41]. These variable results may be due to the long scan times required for precise measurement of v_e [5,46].

It is also worth noting that for our study we used half of the clinical dose of contrast agent. Even with this low contrast agent dose, we detected statistically significant changes in the kinetic DCE metrics between pre- and post-SABR scans and, for K^{trans}, the direction of change was in a consistent direction for all patients. Thus, our results suggest that using a half-dose of contrast agent is sufficient to measure physiological responses to radiotherapy. In a previous study from our group, we investigated the impact of using a lower dose of contrast agent in target volume delineation for radiotherapy planning [20]. We found that using a half clinical dose of contrast agent for target volume delineation in radiotherapy planning did not lead to decreases in the inter- and

intra-observer variability. The combination of the previous study and this study is important in the context of patient safety due to long term retention of gadolinium based contrast agents [47].

There were some limitations to our study. First, our sample size for each group was small limiting statistical power. Even with this limited statistical power, we detected several important changes from pre- to post-SABR MRI scans (changes in K^{trans} for all groups, and changes in v_e, σK^{trans}, and σv_e for some groups as shown in Fig. 3). However, it is possible that some of the pre- to post-SABR comparisons that were not found to be significant here (Fig. 3) could yield significant differences with a larger sample. In addition, our small sample size required the use of nonparametric statistics. In particular, we used a rank-based test, which is not sensitive to the amount of change in parameters from pre to post SABR MRI. Finally, in regards to the small sample size, it was not possible to estimate the population variability for changes in the parameters (e.g., K^{trans}). Second, the comparison between DCE-MRI measurements at approximately 1 week versus 2.5 weeks post-single fraction SABR was based on between-subjects rather than within-subjects comparison. Third, for T_{10} we used an average value over all patients due to difficulties associated with the surgical clip location and the particularly small tumours in two patients. Fourth, we did not image at one-week post-SABR for the 30 Gy/3fraction treatment and cannot determine if surrounding tissue enhancement would occur in this case. Finally, we did not perform pathology-based analysis of the core biopsy and post-surgical tissue to investigate vasculature structure within the tumours and surrounding tissue. In the future, we will continue to accrue patients for investigation from the SIGNAL study. In addition, DCE-MRI with kinetic analysis will be used in a study cur-
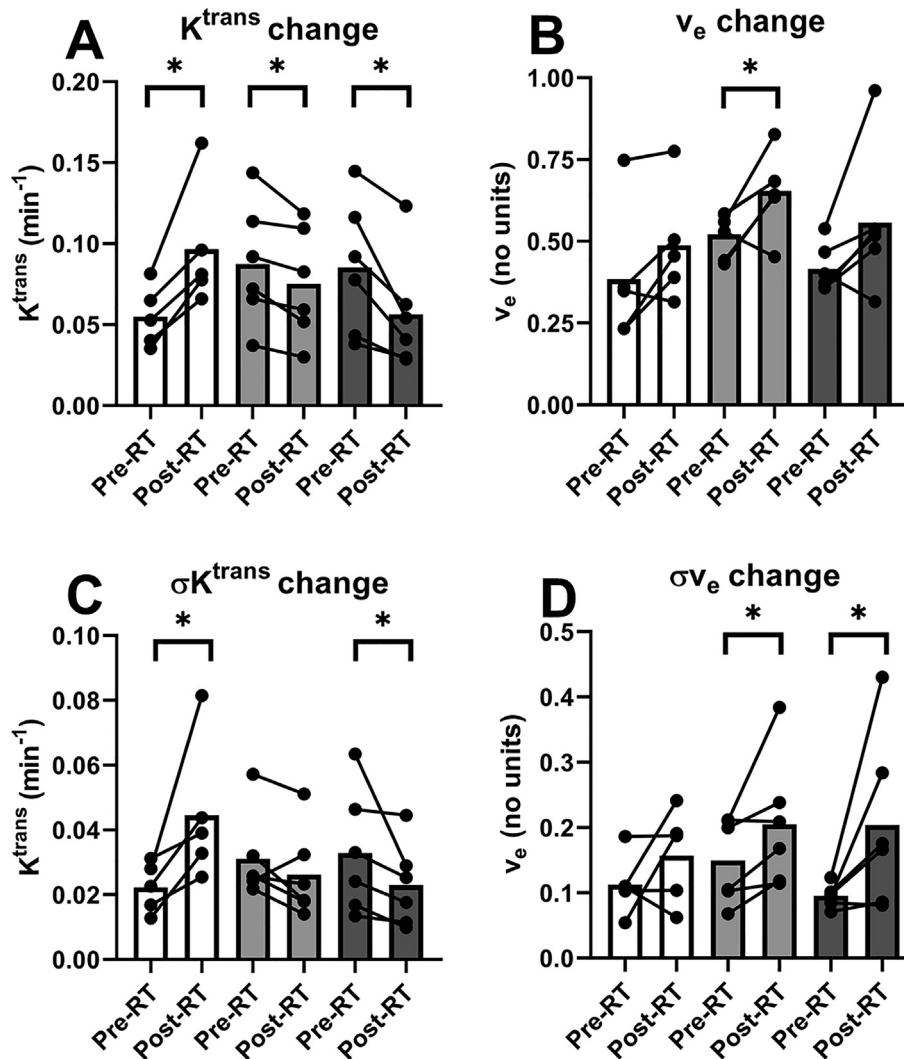
Fig. 3. Pre SBRT vs Post SBRT changes in the mean and standard deviation of kinetic model parameters K^{trans} (A, C) and v_e (B,D) for the three patient groups. These measures refer to the mean and standard deviation over all voxels within the tumor contours of each patient. Circles connected by a line represent an individual patient's pre- and post-SBRT values. The bars represent the median across patients. The asterisks represent significance ($p > 0.05$).

rently being developed at our institution that will be investigating higher risk breast cancer patients undergoing SABR. Early recurrence is more likely in these higher risk patients compared to early stage patient studied here. For this group we will determine the extent to which the kinetic parameter changes from pre- to post-SABR are predictors of patient outcome.

In conclusion, our results demonstrate that our DCE-MRI protocol is sensitive enough to detect a treatment response at approximately 2.5 weeks post SABR. (This protocol utilized ½ of the standard does of contrast agent.) Our results suggest that performing breast DCE-MRI one-week post-SABR may be too early for response assessment – at least for 21 Gy in a single fraction - whereas 2.5 weeks appears sufficiently long to minimize confounding transient acute effects in the tumour. We found that kinetic parameters measured within the tumour at 2.5 weeks post-SABR in both single fraction and three fraction groups were indicative of response, but only the single fraction protocol led to enhancement in the surrounding tissue. While both schemes may lead to similar response within the tumour, no increase in signal enhancement volume from pre- to post- SABR MRI was observed with the three fraction scheme, possibly indicative of a lower radiation impact on surrounding tissue. Longer-term

follow-up of tissue toxicity is needed to confirm this potential benefit of fractionated delivery in this treatment context.

Declaration of Competing Interest

The authors declare that they have no known competing financial interests or personal relationships that could have appeared to influence the work reported in this paper.

References

[1] Njeh CF, Saunders MW, Langton CM. Accelerated Partial Breast Irradiation (APBI): a review of available techniques. Radiat Oncol 2010;5:1–28.

[2] Guidolin K, Lock M, Yaremko B, Gelman N, Gaede S, Kornecki A, et al. A phase II trial to evaluate single-dose stereotactic body radiation therapy (SBRT) prior to surgery for early-stage breast carcinoma: SIGNAL (stereotactic image-guided neoadjuvant ablative radiation then lumpectomy) trial. J Radiat Oncol 2015;4:423–30. https://doi.org/10.1007/s13566-015-0227-2.

[3] Marta GN, Rufino Macedo C, De Andrade Carvalho H, Hanna A, Fernandes Da Silva JL, Riera R. Systematic review Accelerated partial irradiation for breast cancer: Systematic review and meta-analysis of 8653 women in eight randomized trials. Radiother Oncol 2015;114:42–9. https://doi.org/10.1016/j.radonc.2014.11.014.

[4] Nichols E, Kesmodel SB, Bellavance E, Drogula C, Tkaczuk K, Cohen RJ, et al. Preoperative accelerated partial breast irradiation for early-stage breast cancer: preliminary results of a prospective, phase 2 trial. Int J Radiat Oncol Biol Phys 2017;97:747–53. https://doi.org/10.1016/j.ijrobp.2016.11.030.

[5] García-Figueiras R, Goh VJ, Padhani AR, Baleato-González S, Garrido M, León L, et al. CT perfusion in oncologic imaging: a useful tool?. Am J Roentgenol 2013;200:8–19. https://doi.org/10.2214/AJR.11.8476.

[6] Park HJ, Griffin RJ, Hui S, Levitt SH, Song CW, Levitt H, et al. Radiation-Induced Vascular Damage in Tumors: Implications of Vascular Damage in Ablative Hypofractionated Radiotherapy (SBRT and SRS). Radiat Res 2012;177:311–27. https://doi.org/10.1667/RR2773.1.

[7] Wang C-H. Review of treatment assessment using DCE-MRI in breast cancer radiation therapy. World J Methodol 2014;4:46. https://doi.org/10.5662/wjm.v4.i2.46.

[8] Stone HB, Coleman CN, Anscher MS, McBride WH. Effects of radiation on normal tissue: Consequences and mechanisms. Lancet Oncol 2003;4:529–36. https://doi.org/10.1016/S1470-2045(03)01191-4.

[9] Hellevik T, Martinez-Zubiaurre I. Radiotherapy and the tumor stroma: the importance of dose and fractionation. Front Oncol 2014;4:1. https://doi.org/10.3389/fonc.2014.00001.

[10] Milano MT, Constine LS, Okunieff P. Normal tissue toxicity after small field hypofractionated stereotactic body radiation. Radiat Oncol 2008;3. https://doi.org/10.1186/1748-717X-3-36.

[11] Figueiras RG, Padhani AR, Goh VJ, Vilanova JC, Gonzalez SB, Martin CV, et al. Novel oncologic drugs: what they do and how they affect images. Radiographics 2011;31:2059–91. https://doi.org/10.1148/rg.317115108.

[12] Song CW, Kim MS, Cho LC, Dusenbery K, Sperduto PW. Radiobiological basis of SBRT and SRS. Int J Clin Oncol 2014;19:570–8. https://doi.org/10.1007/s10147-014-0717-z.

[13] Wang C, Horton JK, Yin F-F, Chang Z. Assessment of Treatment Response With Diffusion-Weighted MRI and Dynamic Contrast-Enhanced MRI in Patients With Early-Stage Breast Cancer Treated With Single-Dose Preoperative Radiotherapy: Initial Results. Technol Cancer Res Treat 2015. https://doi.org/10.1177/1533034615593191.

[14] Weinmann HJ, Laniado M, Mützel W. Pharmacokinetics of GdDTPA/dimeglumine after intravenous injection into healthy volunteers. Physiol Chem Phys Med NMR 1984;16:167–72.

[15] Othman AE, Falkner F, Kessler D, Martirosian P, Weiss J, Kruck S, et al. Comparison of different population-averaged arterial-input-functions in dynamic contrast-enhanced MRI of the prostate: effects on pharmacokinetic parameters and their diagnostic performance. Magn Reson Imaging 2016;34:496–501. https://doi.org/10.1016/j.mri.2015.12.009.

[16] Patrick JC, Terry Thompson R, So A, Butler J, Faul D, Stodilka RZ, et al. Technical Note: Comparison of megavoltage, dual-energy, and single-energy CT-based μ-maps for a four-channel breast coil in PET/MRI. Med Phys 2017;44:4758–65. https://doi.org/10.1002/mp.12407.

[17] Deoni SCL, Rutt BK, Peters TM. Rapid combined T1 and T2 mapping using gradient recalled acquisition in the steady state. Magn Reson Med 2003;49:515–26. https://doi.org/10.1002/mrm.10407.

[18] Yarnykh VL. Actual flip-angle imaging in the pulsed steady state: a method for rapid three-dimensional mapping of the transmitted radiofrequency field. Magn Reson Med 2007;57:192–200. https://doi.org/10.1002/mrm.21120.

[19] Chung S, Kim D, Breton E, Axel L. Rapid B1+mapping using a preconditioning RF pulse with turboFLASH readout. Magn Reson Med 2010;64:439–46. https://doi.org/10.1002/mrm.22423.

[20] Mouawad M, Biernaski H, Brackstone M, Lock M, Yaremko B, Sexton T, et al. Reducing the dose of gadolinium-based contrast agents for DCE-MRI guided SBRT: the effects on inter and intra observer variability for preoperative target volume delineation in early stage breast cancer patients. Radiother Oncol 2019. https://doi.org/10.1016/j.radonc.2018.11.020.

[21] Johnson HJ, Harris G, Williams K, Williams NK, Williams K. BRAINSFit: Mutual Information Rigid Registrations of Whole-Brain 3D Images, Using the Insight Toolkit. Insight J 2007.

[22] Fedorov A, Beichel R, Kalpathy-Cramer J, Finet J, Fillion-Robin J-C, Pujol S, et al. 3D Slicer as an image computing platform for the Quantitative Imaging Network. Magn Reson Imaging 2012;30:1323–41. https://doi.org/10.1016/j.mri.2012.05.001.

[23] Mattes D, Haynor DR, Vesselle H, Lewellen TK, Eubank W. PET-CT Image Registration in the Chest Using Free-form Deformations. IEEE Trans Med Imaging 2003;22:120–8.

[24] Heinrich MP, Jenkinson M, Bhushan M, Matin T, Gleeson FV, Brady SM, et al. MIND: Modality independent neighbourhood descriptor for multi-modal deformable registration. Med Image Anal 2012;16:1423–35. https://doi.org/10.1016/J.MEDIA.2012.05.008.

[25] Pirozzi S, Kruzer A, Richmond H, Nelson AS. Evaluation of Three Deformable Image Registration Techniques Between CT and CBCT in Prostate Cancer Radiation Therapy. Int J Radiat Oncol 2018;102:e546–7. https://doi.org/10.1016/j.ijrobp.2018.07.1526.

[26] Otsu N. A Threshold Selection Method from Gray-Level Histograms. IEEE Trans Syst Man Cybern 1979;9:62–6. https://doi.org/10.1109/TSMC.1979.4310076.

[27] Gonzalez RC, Woods RE, Masters BR. Digital Image Processing, third ed. vol. 14. 2009. doi: 10.1117/1.3115362.

[28] Celebi ME, Kingravi HA, Vela PA. A comparative study of efficient initialization methods for the k-means clustering algorithm. Expert Syst Appl 2013;40:200–10. https://doi.org/10.1016/j.eswa.2012.07.021.

[29] Reynolds HM, Parameswaran BK, Finnegan ME, Roettger D, Lau E, Kron T, et al. Diffusion weighted and dynamic contrast enhanced MRI as an imaging biomarker for stereotactic ablative body radiotherapy (SABR) of primary renal cell carcinoma. PLoS ONE 2018;13.. https://doi.org/10.1371/journal.pone.0202387.

[30] Pintaske J, Martirosian P, Graf H, Erb G, Lodemann KP, Claussen CD, et al. Relaxivity of gadopentetate dimeglumine (Magnevist), gadobutrol (Gadovist), and gadobenate dimeglumine (MultiHance) in human blood plasma at 0.2, 1.5, and 3 Tesla [published erratum appears in Invest Radiol 2006;41: 859]. Invest Radiol 2006;41:213–21. https://doi.org/10.1097/01.rli.0000197668.44926.f7.

[31] Tofts P, Gunnar B, Buckley DL, Evelhoch JL, Henderson E, Knopp MV, et al. Estimating kinetic parameters from dynamic contrast-enhanced T1-weighted MRI of a diffusable tracer: standardized quantities and symbols. J Magn Reson Imaging 1999;10:223–32.

[32] Parker GJM, Roberts C, Macdonald A, Buonaccorsi GA, Cheung S, Buckley DL, et al. Experimentally-derived functional form for a population-averaged high-temporal-resolution arterial input function for dynamic contrast-enhanced MRI. Magn Reson Med 2006;56:993–1000. https://doi.org/10.1002/mrm.21066.

[33] Leys C, Ley C, Klein O, Bernard P, Licata L. Detecting outliers: Do not use standard deviation around the mean, use absolute deviation around the median. J Exp Soc Psychol 2013;49:764–6. https://doi.org/10.1016/J.JESP.2013.03.013.

[34] Janssen MHM, Aerts HJWL, Kierkels RGJ, Backes WH, Öllers MC, Buijsen J, et al. Tumor perfusion increases during hypofractionated short-course radiotherapy in rectal cancer: sequential perfusion-CT findings. Radiother Oncol 2010;94:156–60. https://doi.org/10.1016/j.radonc.2009.12.013.

[35] Coolens C, Driscoll B, Moseley J, Brock KK, Dawson LA. Feasibility of 4D perfusion CT imaging for the assessment of liver treatment response following SBRT and sorafenib. Adv Radiat Oncol 2016;1:194–203. https://doi.org/10.1016/j.adro.2016.06.004.

[36] Winter JD, Moraes FY, Chung C, Coolens C. Detectability of radiation-induced changes in magnetic resonance biomarkers following stereotactic radiosurgery: A pilot study. PLoS ONE 2018;13. https://doi.org/10.1371/journal.pone.0207933.

[37] Detsky JS, Milot L, Ko Y-J, Munoz-Shuffenegger P, Chu W, Czarnota GJ, et al. Perfusion imaging of colorectal liver metastases treated with bevacizumab and stereotactic body radiotherapy. Phys Imaging Radiat Oncol 2018;5:9–12. https://doi.org/10.1016/j.phro.2018.01.001.

[38] Sawyer B, Pun E, Samuel M, Tay H, Kron T, Bressel M, et al. CT perfusion imaging in response assessment of pulmonary metastases undergoing stereotactic ablative radiotherapy. J Med Imaging Radiat Oncol 2015;59:207–15. https://doi.org/10.1111/1754-9485.12272.

[39] Sen Huang Y, Chen JLY, Hsu FM, Huang JY, Ko WC, Chen YC, et al. Response assessment of stereotactic body radiation therapy using dynamic contrast-enhanced integrated MR-PET in non-small cell lung cancer patients. J Magn Reson Imaging 2018;47:191–9. https://doi.org/10.1002/jmri.25758.

[40] Spratt DE, Arevalo-Perez J, Leeman JE, Gerber NK, Folkert M, Taunk NK, et al. Early magnetic resonance imaging biomarkers to predict local control after high dose stereotactic body radiotherapy for patients with sarcoma spine metastases. Spine J 2016;16:291–8. https://doi.org/10.1016/j.spinee.2015.08.041.

[41] Taunk NK, Oh JH, Shukla-Dave A, Beal K, Vachha B, Holodny A, et al. Early posttreatment assessment of MRI perfusion biomarkers can predict long-term response of lung cancer brain metastases to stereotactic radiosurgery. Neuro Oncol 2018;20:567–75. https://doi.org/10.1093/neuonc/nox159.

[42] Brown SL, Nagaraja TN, Aryal MP, Panda S, Cabral G, Keenan KA, et al. MRI-Tracked Tumor Vascular Changes in the Hours after Single-Fraction Irradiation. Radiat Res 2015;183:713–21. https://doi.org/10.1667/rr13458.1.

[43] Venkatesulu BP, Mahadevan LS, Aliru ML, Yang X, Bodd MH, Singh PK, et al. Radiation-Induced Endothelial Vascular Injury. JACC Basic Transl Sci 2018;3:563–72. https://doi.org/10.1016/j.jacbts.2018.01.014.

[44] Cao Y. The Promise of Dynamic Contrast-Enhanced Imaging in Radiation Therapy. Semin Radiat Oncol 2011;21:147–56. https://doi.org/10.1016/j.semradonc.2010.11.001.

[45] Barker HE, Paget JTEE, Khan AA, Harrington KJ. The tumour microenvironment after radiotherapy: mechanisms of resistance and recurrence. Nat Publ Gr 2015;15:409–25. https://doi.org/10.1038/nrc3958.

[46] Tofts PS, Parker GJM. DCE-MRI: Acquisition and analysis techniques. In: Barker P, Golay X, Zaharchuk G, editors. Clin. Perfus. MRI Tech. Appl.. Cambridge: Cambridge University Press; 2010. p. 58–74. vol. 9781107013, doi: 10.1017/CBO9781139004053.006.

[47] Gulani V, Calamante F, Shellock FG, Kanal E, Reeder SB. Gadolinium deposition in the brain: summary of evidence and recommendations. Lancet Neurol 2017;16:564–70. https://doi.org/10.1016/S1474-4422(17)30158-8.